Global dynamical analysis of vibrational manifolds of HOCl and HOBr under anharmonicity and Fermi resonance: the dynamical potential approach*

Fang Chao(房 超) and Wu Guo-Zhen(吴国祯)†

Molecular and Nano Sciences Laboratory, Department of Physics, Tsinghua University, Beijing 100084, *China*

(Received 19 May 2009; revised manuscript received 18 June 2009)

The vibrational dynamics of HOCl and HOBr between bending and OCl/OBr stretching coordinates with anharmonicity and Fermi coupling is studied with the classical dynamical potential approach. The quantal vibrational dynamics is mostly mapped out by the classical nonlinear variables such as fixed points, except for the state energies, which are quantized. This approach is global in the sense that the focus is on a set of levels instead of individual ones. The dynamics of HOBr is demonstrated to be less complicated. The localized modes along the OCl/OBr stretching coordinates are also shown to have O–Br bonds more prone to dissociation.

Keywords: HOCl/HOBr, dynamical potential, Fermi coupling, global dynamics

PACC: 0545M, 3115Q

1. Introduction

The vibrational dynamics of HOCl and HOBr between bending and OCl/OBr stretching coordinates with anharmonicity and Fermi couplings has been studied[1−8] by the quantal *ab initio* calculation and classical bifurcational analysis. In our previous work[9] on similar systems of HCP (phosphaethyne) and DCP (deuterated phosphaethyne), the vibrational dynamics has been successfully approached by another algorithm: the dynamical potential in the coset phase space based on an algebraic (spectroscopic) Hamiltonian. In fact, dynamical potential is the effective potential the nuclear coordinates experience, dynamically. This approach shows its superiority in that it is very simple and shows a clear picture, both methodically and physically. The fixed points shown in the dynamical potentials are easily identified to govern the various quantal environments in which the vibrational states lie. The state dynamics is interpreted by classical actions which are easily calculated by this algorithm. Also, state classification is realized by action integrals. Localized modes which are robust against intramolecular vibrational relaxation (IVR) even at high excitation are also easily identified.

With this idea, hereby, we report on the study of the vibrational systems of HOCl and HOBr. In these integrable systems, the quantal states are found to be imbedded in the dynamical potential which are characterized by fixed points. In other words, the quantal vibrational dynamics is mostly mapped out by classical nonlinear variables except for the state energies, which are quantized. This approach is global in the sense that the focus is on a set of levels instead of individual ones. By this classical algorithm, the dynamics of HOBr is demonstrated to be simpler. The localized modes along the OCl/OBr stretching coordinates are also shown to have O–Br bonds more prone to dissociation.

2. Coset space represented Hamiltonians

The algebraic Hamiltonians of HOCl and HOBr including their coefficients have been determined in Refs. [1] and [8] by fitting the eigenenergies of this Hamiltonian (with quantized actions) to those levels obtained from the exact quantum calculation. For notation, the subscripts 1, 2 and 3 denote H–O stretch, H–O–Cl/H–O–Br bend and O–Cl/O–Br stretch respectively; n, ω, X, y and z represent action, linear and nonlinear coefficients respectively; k's refer to the Fermi resonance; a^+ and a are the creation and the destruction operators. For reference, they are summarized in Table 1.

*Project supported by the Research Foundation from Ministry of Education of China (Grant No. 306020), the Specialized Research Fund for the Doctoral Program of Higher Education, China (Grant No. 20060003050), and the National Natural Science Foundation of China (Grant No. 20373030).

†Corresponding author. E-mail: wgz-dmp@tsinghua.edu.cn

© 2010 Chinese Physical Society and IOP Publishing Ltd

Table 1. Coefficients for HOCl and HOBr algebraic Hamiltonians.

parameter/cm^{-1}	HOCl	HOBr	parameter/cm^{-1}	HOCl	HOBr	parameter/cm^{-1}	HOCl	HOBr
ω_1	3777.067	3769.5381	y_{133}	–0.0532	–0.9150	y_{11122}	0	0.257802
ω_2	1258.914	1187.7106	y_{223}	–0.0802	–0.6071	y_{11222}	0	0.257802
ω_3	753.834	622.3722	y_{233}	0.2503	0	y_{11223}	0	0.032641
X_{11}	–80.277	–70.7877	y_{1133}	0	0.203607	y_{12222}	0	–0.020228
X_{22}	–3.204	–5.4432	y_{2222}	–0.04117	0	y_{22333}	–0.00066	–0.001709
X_{33}	–7.123	–3.5507	y_{1333}	0	0.0121098	y_{22233}	0	0.003254
X_{12}	–19.985	–26.8651	y_{3333}	0.00171	–0.000603	k	0	0
X_{13}	0	10.3315	y_{1122}	–0.15070	0	k_1	0	0.8717
X_{23}	–10.637	–3.7702	y_{1222}	0.13189	0	k_2	–0.76017	–0.3183
y_{111}	–0.3619	0	y_{2333}	–0.01229	–0.001461	k_3	–0.24939	–0.1935
y_{113}	0	–3.4216	y_{1233}	0.02381	0	k_{22}	–0.01158	–0.016988
y_{333}	0.0825	0	y_{22222}	0.00151	0	k_{23}	0.04075	0
y_{122}	–1.9534	–1.1955	y_{11112}	0	–0.656865	k_{33}	0.00583	0

The algebraic Hamiltonian is in the following form:

$$
\begin{aligned}
H = {} & \omega_1\left(n_1+\frac{1}{2}\right)+\omega_2\left(n_2+\frac{1}{2}\right)+\omega_3\left(n_3+\frac{1}{2}\right)+X_{11}\left(n_1+\frac{1}{2}\right)^2+X_{22}\left(n_2+\frac{1}{2}\right)^2+X_{33}\left(n_3+\frac{1}{2}\right)^2 \\
& +X_{12}\left(n_1+\frac{1}{2}\right)\left(n_2+\frac{1}{2}\right)+X_{23}\left(n_2+\frac{1}{2}\right)\left(n_3+\frac{1}{2}\right)+X_{13}\left(n_1+\frac{1}{2}\right)\left(n_3+\frac{1}{2}\right) \\
& +y_{111}\left(n_1+\frac{1}{2}\right)^3+y_{113}\left(n_1+\frac{1}{2}\right)^2\left(n_3+\frac{1}{2}\right)+y_{333}\left(n_3+\frac{1}{2}\right)^3+y_{122}\left(n_1+\frac{1}{2}\right)\left(n_2+\frac{1}{2}\right)^2 \\
& +y_{133}\left(n_1+\frac{1}{2}\right)\left(n_3+\frac{1}{2}\right)^2+y_{223}\left(n_2+\frac{1}{2}\right)^2\left(n_3+\frac{1}{2}\right)+y_{233}\left(n_2+\frac{1}{2}\right)\left(n_3+\frac{1}{2}\right)^2 \\
& +y_{1133}\left(n_1+\frac{1}{2}\right)^2\left(n_3+\frac{1}{2}\right)^2+y_{2222}\left(n_2+\frac{1}{2}\right)^4+y_{1333}\left(n_1+\frac{1}{2}\right)\left(n_3+\frac{1}{2}\right)^3+y_{3333}\left(n_3+\frac{1}{2}\right)^4 \\
& +y_{1122}\left(n_1+\frac{1}{2}\right)^2\left(n_2+\frac{1}{2}\right)^2+y_{1222}\left(n_1+\frac{1}{2}\right)\left(n_2+\frac{1}{2}\right)^3+y_{2333}\left(n_2+\frac{1}{2}\right)\left(n_3+\frac{1}{2}\right)^3 \\
& +y_{1233}\left(n_1+\frac{1}{2}\right)\left(n_2+\frac{1}{2}\right)\left(n_3+\frac{1}{2}\right)^2+y_{22222}\left(n_2+\frac{1}{2}\right)^5+y_{11112}\left(n_1+\frac{1}{2}\right)^4\left(n_2+\frac{1}{2}\right) \\
& +y_{11122}\left(n_1+\frac{1}{2}\right)^3\left(n_2+\frac{1}{2}\right)^2+y_{11222}\left(n_1+\frac{1}{2}\right)^2\left(n_2+\frac{1}{2}\right)^3+y_{11223}\left(n_1+\frac{1}{2}\right)^2\left(n_2+\frac{1}{2}\right)^2\left(n_3+\frac{1}{2}\right) \\
& +y_{12222}\left(n_1+\frac{1}{2}\right)\left(n_2+\frac{1}{2}\right)^4+y_{22333}\left(n_2+\frac{1}{2}\right)^2\left(n_3+\frac{1}{2}\right)^3+y_{22233}\left(n_2+\frac{1}{2}\right)^3\left(n_3+\frac{1}{2}\right)^2 \\
& +\left[k+k_1\left(n_1+\frac{1}{2}\right)+k_2n_2+k_3\left(n_3+\frac{3}{2}\right)+k_{22}n_2^2+k_{23}n_2\left(n_3+\frac{3}{2}\right)+k_{33}\left(n_3+\frac{3}{2}\right)^2\right](a_2^+a_3^2+a_3^{+2}a_2).
\end{aligned}
$$

This Hamiltonian is semiclassical in the sense that it is based on the model of coupled Morse oscillators with Fermi resonance between the bend and O–Cl/O–Br stretch which is described by the second quantization operators. n_1 is usually treated as a fixed integer because the couplings between the H–O stretching and the rest coordinates are very weak.

Significantly, for these two Hamiltonians, besides n_1, there is another conserved action, called the polyad number, $P = 2n_2 + n_3$. P is limited to 30 due to the fact that these coefficients are determined by fitting to the state energies with $P \leq 30$.

For further semiclassical treatment, the Heisenberg correspondence[10] is used to transform the second quantization operators to classical quantities. Mathematically, this is equivalent to transforming to the coset space.[11] The coset space is a phase space for the vibrational dynamics. This transformation is accomplished through the substitution of $n_2 = (q_2^2 + p_2^2)/2$ for constants n_1 (which will be set to 0 in our study) and P. Thus, $n_3 = P - (q_2^2 + p_2^2)$. The coset space represented Hamiltonian is

$$
\begin{aligned}
H(q_2,p_2,P) = {} & \frac{1}{2}\omega_1 + \omega_2\left(\frac{p_2^2+q_2^2}{2}+\frac{1}{2}\right) + \omega_3\left(P-(p_2^2+q_2^2)+\frac{1}{2}\right) + \frac{1}{4}X_{11} \\
& + X_{22}\left(\frac{p_2^2+q_2^2}{2}+\frac{1}{2}\right)^2 + X_{33}\left(P-(p_2^2+q_2^2)+\frac{1}{2}\right)^2 + \frac{1}{2}X_{12}\left(\frac{p_2^2+q_2^2}{2}+\frac{1}{2}\right) \\
& + X_{23}\left(\frac{p_2^2+q_2^2}{2}+\frac{1}{2}\right)\left(P-(p_2^2+q_2^2)+\frac{1}{2}\right) + \frac{1}{2}X_{13}\left(P-(p_2^2+q_2^2)+\frac{1}{2}\right) + \frac{1}{8}y_{111} \\
& + \frac{1}{4}y_{113}\left(P-(p_2^2+q_2^2)+\frac{1}{2}\right) + y_{333}(P-(p_2^2+q_2^2)+\frac{1}{2})^3 + \frac{1}{2}y_{122}\left(\frac{p_2^2+q_2^2}{2}+\frac{1}{2}\right)^2 \\
& + \frac{1}{2}y_{133}\left(P-(p_2^2+q_2^2)+\frac{1}{2}\right)^2 + y_{223}\left(\frac{p_2^2+q_2^2}{2}+\frac{1}{2}\right)^2\left(P-(p_2^2+q_2^2)+\frac{1}{2}\right) \\
& + y_{233}\left(\frac{p_2^2+q_2^2}{2}+\frac{1}{2}\right)\left(P-(p_2^2+q_2^2)+\frac{1}{2}\right)^2 + \frac{1}{4}y_{1133}\left(P-(p_2^2+q_2^2)+\frac{1}{2}\right)^2 \\
& + y_{2222}\left(\frac{p_2^2+q_2^2}{2}+\frac{1}{2}\right)^4 + \frac{1}{2}y_{1333}\left(P-(p_2^2+q_2^2)+\frac{1}{2}\right)^3 + y_{3333}\left(P-(p_2^2+q_2^2)+\frac{1}{2}\right)^4 \\
& + \frac{1}{4}y_{1122}\left(\frac{p_2^2+q_2^2}{2}+\frac{1}{2}\right)^2 + \frac{1}{2}y_{1222}\left(\frac{p_2^2+q_2^2}{2}+\frac{1}{2}\right)^3 + y_{2333}\left(\frac{p_2^2+q_2^2}{2}+\frac{1}{2}\right)\left(P-(p_2^2+q_2^2)+\frac{1}{2}\right)^3 \\
& + \frac{1}{2}y_{1233}\left(\frac{p_2^2+q_2^2}{2}+\frac{1}{2}\right)\left(P-(p_2^2+q_2^2)+\frac{1}{2}\right)^2 + y_{22222}\left(\frac{p_2^2+q_2^2}{2}+\frac{1}{2}\right)^5 \\
& + \frac{1}{16}y_{11112}\left(\frac{p_2^2+q_2^2}{2}+\frac{1}{2}\right) + \frac{1}{8}y_{11122}\left(\frac{p_2^2+q_2^2}{2}+\frac{1}{2}\right)^2 + \frac{1}{4}y_{11222}\left(\frac{p_2^2+q_2^2}{2}+\frac{1}{2}\right)^3 \\
& + \frac{1}{4}y_{11223}\left(\frac{p_2^2+q_2^2}{2}+\frac{1}{2}\right)^2\left(P-(p_2^2+q_2^2)+\frac{1}{2}\right) + \frac{1}{2}y_{12222}\left(\frac{p_2^2+q_2^2}{2}+\frac{1}{2}\right)^4 \\
& + y_{22333}\left(\frac{p_2^2+q_2^2}{2}+\frac{1}{2}\right)^2\left(P-(p_2^2+q_2^2)+\frac{1}{2}\right)^3 + y_{22233}\left(\frac{p_2^2+q_2^2}{2}+\frac{1}{2}\right)^3\left(P-(p_2^2+q_2^2)+\frac{1}{2}\right)^2 \\
& + \left[k + \frac{1}{2}k_1 + k_2\frac{p_2^2+q_2^2}{2} + k_3\left(P-(p_2^2+q_2^2)+\frac{3}{2}\right) + k_{22}\left(\frac{p_2^2+q_2^2}{2}\right)^2\right. \\
& \left. + k_{23}\frac{p_2^2+q_2^2}{2}\left(P-(p_2^2+q_2^2)+\frac{3}{2}\right) + k_{33}\left(n_3+\frac{3}{2}\right)^2\right]\sqrt{2}(P-(p_2^2+q_2^2))q_2.
\end{aligned}
$$

The corresponding equations of motion are: $\partial H/\partial q_2 = -\mathrm{d}p_2/\mathrm{d}t$, and $\partial H/\partial p_2 = \mathrm{d}q_2/\mathrm{d}t$. This provides our tools for the dynamical analysis of this highly excited vibrational system.

Similarly, we can have $H(q_3,\ p_3)$ and the corresponding equations of motion.

3. Dynamical potentials, fixed points, action populations, action percentages and action integrals

The dynamical potential[12,13] of $H(q_i,\ p_i,\ P)$ is the effective environment in which the q_i coordinate stays for each P. This is achieved by calculating the maximal and minimal energies by varying p_i for each q_i on condition that n_2 and n_3 are nonnegative. The dynamical potential composed of these maximal and minimal energies as a function of q_i is represented by a closed curve in which the quantal levels are enclosed. The dynamical potential also defines the q_i region for each level it encloses. The points of the dynamical potential correspond to $\partial H/\partial p_i = 0$. Furthermore, the points in the dynamical potential corresponding to $\partial H/\partial q_i = 0$ are fixed points in the dynamical space. Therefore, at these fixed points, both n_2 and $n_3/2$ are time invariant. So, the fixed points we mean here are those on which the actions are constant in this dynamical system. These fixed points will be denoted by B if it is mainly of bending character and R if it is mainly of O–Cl/O–Br stretching character. A solid (open) star is for the second stable (unstable) B and R. An additional number 2 or 3 is attached as a reminder of their appearance in the dynamical potential in q_2 or q_3 coordinate. Bars above B and R are for the unstable fixed points. (The actions on these fixed points are calculated by $n_2 = (q_2^2+p_2^2)/2$ and $n_3 = P-(q_2^2+p_2^2)$

or $n_3 = (q_3^2 + p_3^2)/2$, $n_2 = P/2 - (q_3^2 + p_3^2)/4$ in the $H(q_3,\ p_3)$ representation.) We will note that the dynamical potential is mainly composed of two portions with the lower one, more or less, like a (deformed) Morse well and the upper one like an inverse Morse well. Hence, for the upper realm of the dynamical potential, we need to interpret the potential curve in an inverse (upside down) way.

For each level, in the allowed q_i region, p_i can be known (from $H(q_i,\ p_i)$) and so can n_2 and $n_3/2$. These quantities, n_2 and $n_3/2$, each as a function of q_i, can be interpreted as the action populations in the dynamical coset space for a level. These quantities are analogues of the wave function density in the quantal treatment. We may further obtain the action percentages for each level by integrating n_2 and $n_3/2$, separately, through the allowed q_i coordinate and setting their values in percentage. (These action percentages are independent of the coordinate q_2 or q_3 used.)

For each level, we can calculate the trajectories via eigenenergy $= H(q_i,\ p_i)$ in the coset spaces. The trajectories are closed contours for each level since the system is integrable. We can calculate the corresponding action integrals

$$1/2\pi \oint p_i \mathrm{d}q_i$$

along the contour in the $(q_2,\ p_2)$ and $(q_3,\ p_3)$ spaces. We will see that these action integrals reflect the very essential properties of the levels imbedded in the dynamical potential.

These quantities—the dynamical potential, fixed point, action population, action percentage and action integral—are the tools we will employ for the dynamical analysis. We will see that with these quantities, a great deal of information about the vibrational dynamics can be obtained, thereby showing that this method is comparable to the traditional Schroedinger wave function approach. In other words, the background of the quantal properties is, in fact, the classical nonlinear variables, of which the fixed points are the core.

4. HOCl system

The levels of the HOCl system are shown in Fig. 1(a). These levels are grouped by the polyad number P. Shown therein are also the fixed points whose appearance will be apparent from the corresponding dynamical potentials which are shown in Fig. 2(a). From the appearance of the fixed points, the levels are grouped into five categories with the polyad number P being 10–18, 20, 22, 24 and 26–30. We note that the dynamical structure changes most when the polyad number is around 20, 22 and 24. For the levels below and above these energy realms, the dynamical structure remains quite unchanged.

Shown in Fig. 2(a) are the dynamical potentials in q_2 and q_3 coordinates with P being 12, 20, 22, 24 and 30 for displaying the dynamical structural characters of the five categories. The horizontal lines shown therein denote the quantized levels. We note that quantized levels sharing a common polyad number are enclosed in their respective dynamical potential. Also shown are the fixed points. The lower portion of the dynamical potential is of (deformed and even multiple) Morse type while the upper portion is of an inverse (deformed and even multiple) Morse type. How impressive it is that the nearest level spacing around the top of the Morse well or the bottom of the inverse Morse well is usually narrower. These regions correspond to the dynamical separatrix and often therefrom the unstable fixed points come into being. This is most evident in the case where the values of P are 24 and 30. The narrowing of the nearest level spacing would be difficult to understand without the dynamical potential. We further note that the dynamical potentials with $P = 24$ are very similar to those of HCP with $P = 22$ though with the q_2 and q_3 coordinates swapped.[9] The property of bending localization in HCP[14] is therefore expected to be reflected in the localization of the O–Cl stretching mode in this HOCl system.

Shown in Fig. 2(a) are also the action percentages for the corresponding levels. The levels are numbered from the highest to the lowest as L0 to L($P/2$) for each P. For small P, the higher levels possess more actions in the O–Cl stretching coordinate and the lower levels possess more actions in the H–O–Cl bending coordinate. As P reaches 24, an abrupt change occurs where the very low levels possess localized actions in the O–Cl coordinate. As mentioned, this localization of action was observed in the HCP bending coordinate[9] also. We note that these two cases of action localization share a common character in their dynamical potentials. The character is that localization occurs in the levels which possess an interval centred around nonzero q_i just above a stable fixed point in the dynamical potential. This is indeed a very convenient way of predicting the levels that possess action localization. This is further demonstrated in the action populations.

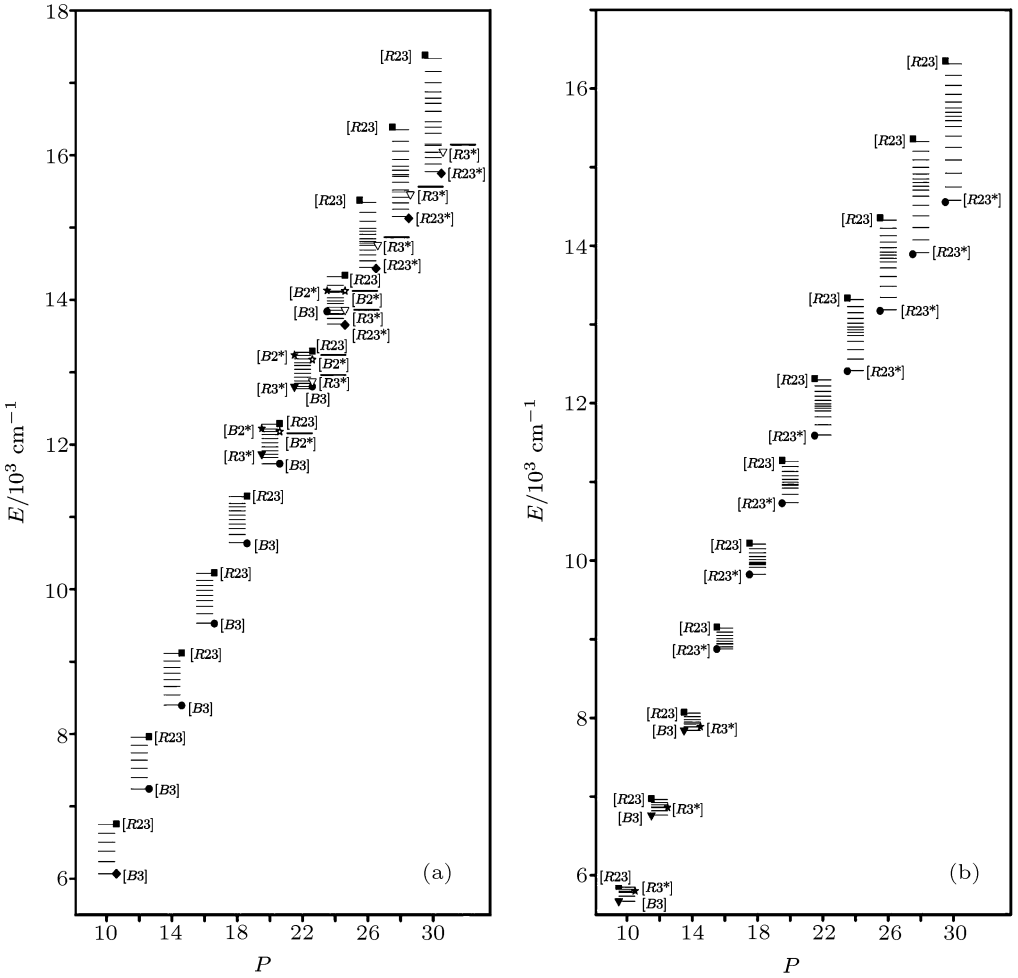
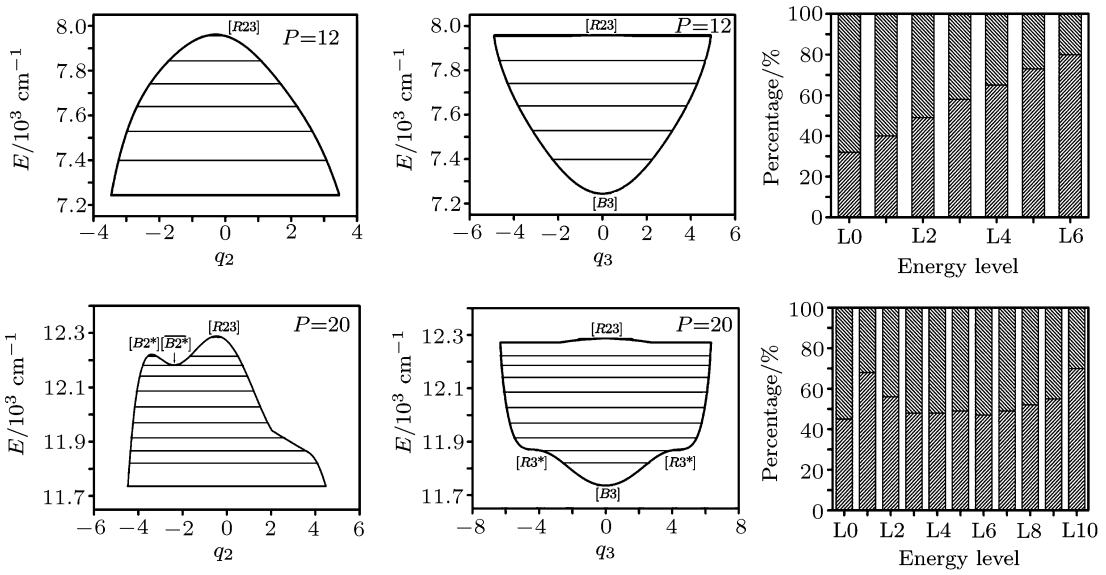


Fig. 1. Levels for various values of P (up to 30) for (a) HOCl and (b) HOBr. Their state energies are relative to the zero point energies which are 2864.2 cm^{-1} and 2764.0 cm^{-1}, respectively, above the potential well bottoms. Also shown are the fixed points. The notations are B for the bending character, R for the O–Cl stretching character, solid (open) star for the second stable (unstable) B and R. Numbers 2 and 3 are for their appearances in the dynamical potentials at q_2 and q_3 coordinates, respectively. Bars above B and R are for the unstable fixed points. See text for details.



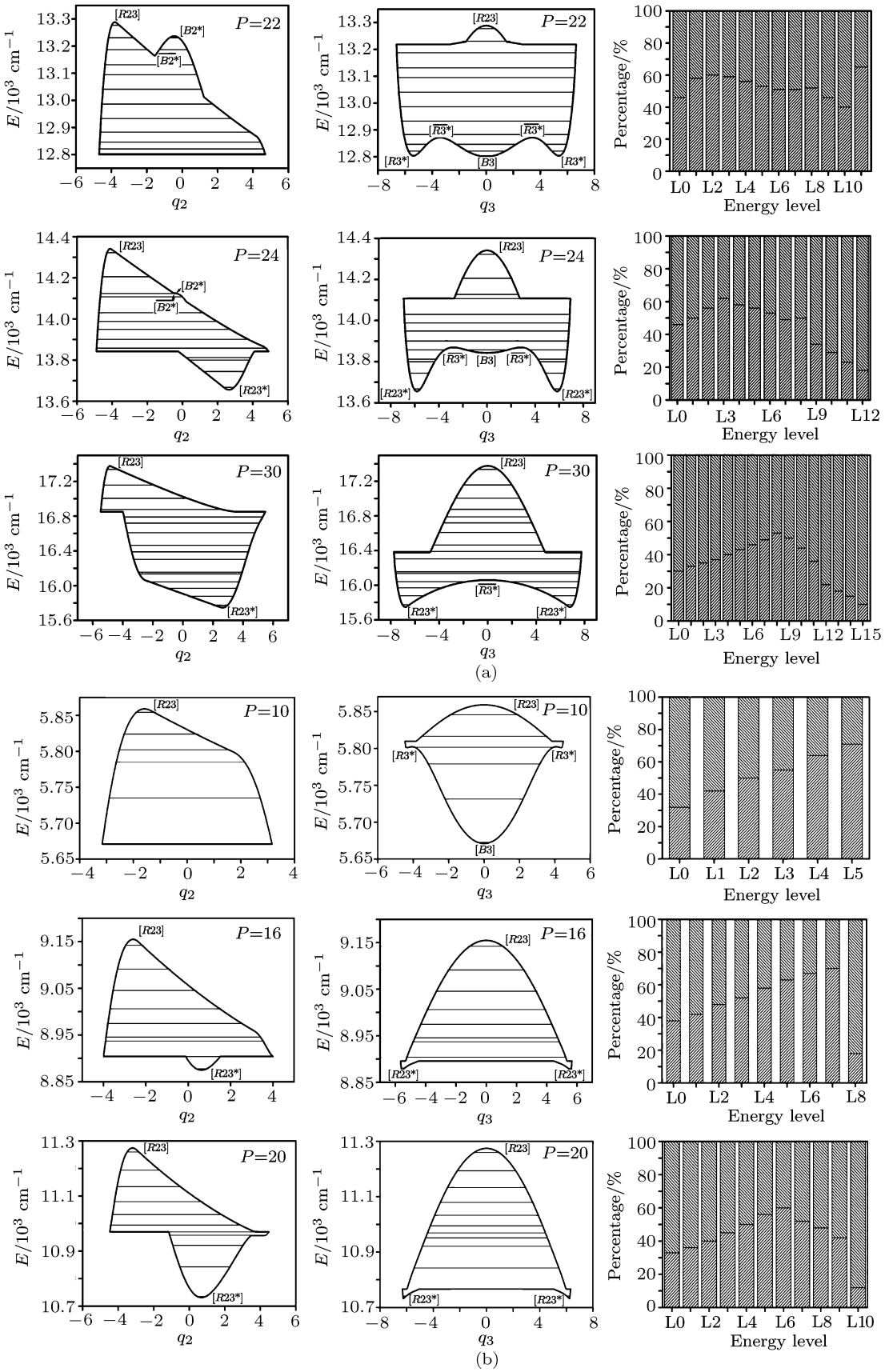


Fig. 2. Dynamical potentials and levels imbedded therein for (a) HOCl (b) HOBr under various polyad numbers and the action percentages of n_2 (right-up shadow) and $n_3/2$ (left-up shadow) for the respective levels. Note that the levels are numbered from the highest to the lowest as L0 to L($P/2$) for each P. Also shown are the fixed points. See caption of Fig.1 for the notation. See text for details.

Shown in Fig.3 (a) are n_2 and $n_3/2$, each as a function of q_2 for the levels with $P = 30$, for demonstration. (Those, each as a function of q_3, offer identical conclusions.) The localization of actions is observed in the lowest four levels, L12–L15, for which $n_3/2$ is always larger than n_2.

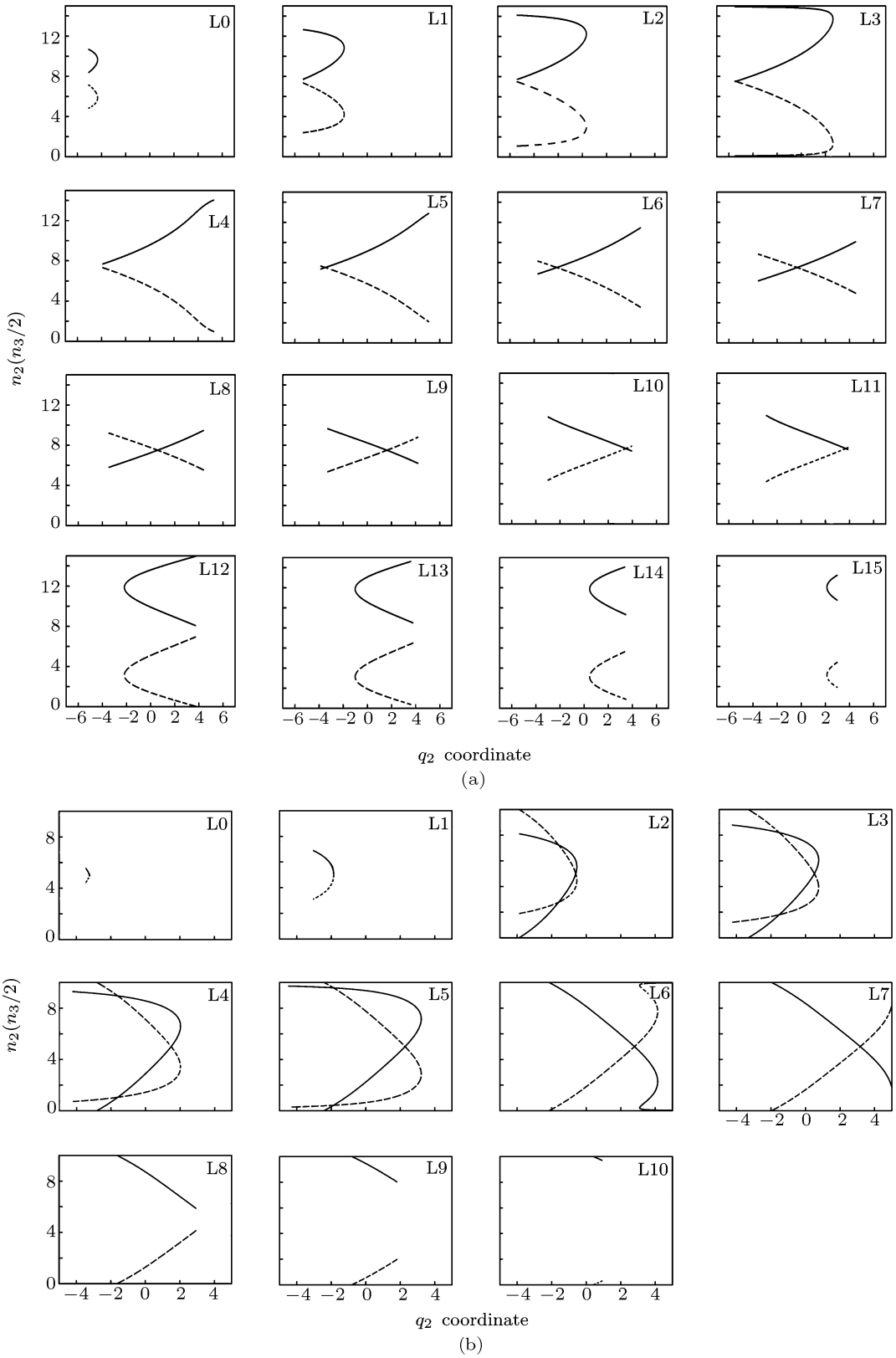


Fig. 3. Action populations as a function of q_2 coordinate for the levels with $P = 30$ for HOCl (a) and $P = 20$ for HOBr (b). The solid line is for $n_3/2$ and the broken line is for n_2.

For the higher levels from L0 to L4, though $n_3/2$ is also larger than n_2, the action interchange between the q_2 and q_3 coordinates is eminently more violent than that in L12–L15. For the levels in between, IVR (intramolecular vibrational relaxation) between bending and O–Cl stretching is rather complete. (See the cross-over of the n_2 and $n_3/2$ curves.) These level characters are identical to those by the quantal wave functions, except that the quantal calculation indicates that L10, L12[4] (or L11, L13[1]) are drastically more of bending character, unlike their neighbouring levels. In fact, this discrepancy is not fatal. We note that these levels are very close to the unstable fixed point $[\overline{R3^*}]$ so that if the motion stays on it ($q_3 = 0$), the action (energy) will be mostly localized on the bending coordinate just as that evidenced by the quantal calculation. This discrepancy is found in the levels close to the unstable fixed points, in general. This will be also found in the HOBr case. In fact, this is the scarring effect by Heller[15] that there is enhancement of the wave function amplitude around the unstable periodic orbits.

The action integrals for the levels sharing a common polyad number are useful in categorizing the level character. The case for $P = 30$ is shown in Table 2. Indeed, we note that for the levels from the highest one down in the upper region (which is of an inverse Morse type) of the dynamical potential in either q_2 or q_3 coordinate, the action integral increases by a constant increment. This corresponds to the character of an inverse Morse type potential, while for the levels from the lowest one up, the action integral increases by a constant increment, corresponding to a Morse type potential. We note that the interpretation of the level property from the dynamical potential and that by the action integral are two independent approaches which both lead to a consistent conclusion.

Before drawing the conclusion from the HOCl case study, we note that action localization occurs only in the O–Cl bond but not on the bending motion. This is contrary to the HCP case. Therefore, we access that the isomerization to HClO through the internal rotation of H atom is rather difficult, unlike that of HCP. Instead, the dissociation of the O–Cl bond is more prone to occur from the viewpoint of action (energy) localization.

Table 2. (a) Action integrals of 16 quantal states corresponding to $P = 30$ for HOCl and (b) those of the states corresponding to $P = 20$ for HOBr.

state label	action integral in (q_2p_2) space	difference of the action integrals between the neighbouring levels	action integral in (q_3p_3) space	difference of the action integrals between the neighbouring levels
L0	0.3	/	0.3	/
L1	1.4	1.1	2.0	1.7
L2	2.5	1.1	3.9	1.9
L3	3.5	1.0	5.9	2
L4	11.1	/	7.7	1.8
L5	10.2	–0.9	9.6	1.9
L6	9.3	–0.9	11.5	1.9
L7	8.3	–1.0	13.3	1.8
L8	7.4	–0.9	16.0	/
L9	6.3	–1.1	14.0	–2.0
L10	5.3	–1.0	11.8	–2.2
L11	4.2	–1.1	9.4	–2.4
L12	3.4	–0.8	7.2	–2.2
L13	2.4	–1.0	4.9	–2.3
L14	1.2	–1.2	2.6	–2.3
L15	0.2	–1.0	0.3	–2.3

Table 2. (b)

state label	action integral in (q_2p_2) space	difference of the action integrals between the neighbouring states	action integral in (q_3p_3) space	difference of the action integrals between the neighbouring states
L0	0.3	/	0.3	/
L1	1.2	0.9	2.2	1.9
L2	2.3	1.1	4.3	2.1
L3	3.3	1.0	6.3	2.0
L4	4.3	1.0	8.1	1.8
L5	5.5	1.2	10.1	2.0
L6	5.0	/	12.2	2.1
L7	3.9	–1.1	14.0	1.8
L8	2.6	–1.3	16.0	2.0
L9	1.5	–1.1	18.1	2.1
L10	0.3	–1.2	0.3	/

5. HOBr system

The previous study on the HOCl system offers us a routine analysis for the HOBr case. Shown in Fig. 1(b) is the energy diagram from $P = 10$ up to 30 together with the fixed points which are more obvious from the dynamical potentials as shown in Fig. 2(b). From the fixed point structure, the vibrational dynamics can be grouped into two categories: $P = 10$ to 14, 16–30. (The dynamical potential in the q_2 coordinate for $P = 16$ shows uniqueness and is also shown in Fig. 2(b).)

The general structure of the dynamical potentials is composed of an inverse Morse well in the upper energy realm and one (or two) Morse one(s) in the lower energy realm. The nearest neighbouring energy spacing becomes the smallest around where the inverse Morse well and Morse well join together. This corresponds to the dynamical separatrix. The fixed point structure of the HOBr system shows that it possesses much simpler dynamics than the HOCl system. Also noted is that bending character disappears for levels with larger P. This was also confirmed in Ref. [8].

Also shown in Fig. 2(b) are the action percentages of the respective levels. The action localization in the O–Br coordinate is observed in those lowest levels for $P = 16$ up to 30. These levels also possess the property that, in the dynamical potentials, they are localized in a region centred around nonzero q_i just above a stable fixed point. This is the same as what happens to the HOCl system. The localization phenomenon starts emerging for smaller polyad numbers than those in the HOCl system. This is suggested to be related to the easier dissociation of the O–Br bond than the O–Cl bond.

The quantal wave function analysis shown in Ref. [8] for $P = 20$ indicates that the lowest three levels are more populated along the O–Br motion and that higher levels show full resonance between the bending and the O–Br modes. It is consistent with our study as shown in Fig. 3(b) that, for the lowest three levels, $n_3/2$ is always larger than n_2 and that, for higher levels, the curves of $n_3/2$ and n_2 cross over, showing IVR between the bending and the O–Br modes. However, L7 is localized along the bending coordinate as shown by its quantal wave function. Again, L7 is close to the unstable flat region of the dynamical potential in the q_2 coordinate as shown in Fig. 2(b). Therefore, for this level, if the motion stays fixed on the large q_2 coordinate, it will be mainly along the bending coordinate. So, this subtlety predicted by the quantal calculation can be reasoned by the fact that this level is near the unstable region in classical dynamical space.

The action integrals for the levels with $P = 20$ are shown in Table 2(b). In the $(q_2,\ p_2)$ space, for the higher levels in the upper inverse Morse well, the action integral increases from the top level down by a constant increment. For the lower levels, the action integral increases from the lowest level up by a constant increment, showing a Morse well character. In the $(q_3,\ p_3)$ space, except for the lowest level, all the action integrals show the behaviour of an inverse Morse well in which the levels are imbedded. The consistent implications of the action integral and the dynamical potential are well established.

6. Concluding remarks

The vibrational dynamics of HOCl and HOBr between the bending and OCl/OBr stretching coordinates with anharmonicity and Fermi coupling is studied with the classical dynamical potential approach. In these integrable systems, the quantal states are found to be imbedded in the dynamical potentials which are characterized by the fixed points. The dynamical potential is mainly composed of (deformed) inverse Morse and Morse wells. In other words, the quantal states stay in the multiple environments of the dynamical potential, which can be employed for state classification. This is confirmed by the classical action integrals. The classical analysis also employs the action distribution (population and percentage). This classical analysis can lead to most inferences drawn by the quantal wave function algorithm. The subtle behaviour of the state wave functions that show drastic change of mode character in a set of states sharing a common polyad number is found to be related to the unstable region/fixed point in the dynamical space. By this classical algorithm, the dynamics of HOBr is demonstrated to be less complicated than that of HOCl.

The action localization in the O–Cl/O–Br coordinates is observed in the levels that possess an interval centred around nonzero q_i just above a stable fixed point in the dynamical potential. The localization analysis demonstrates that the O–Br bond is more prone to dissociation than the O–Cl bond.

This approach is global in the sense that the focus is on a set of levels instead of individual ones. The significance of this work is that the main theme of this vibrational dynamics can be mostly mapped out by classical nonlinear variables except the state energies that are quantized.

Finally, it should be noted that our approach is but one branch in the field of algebraic approaches to molecular vibrational dynamics. Others like Refs. [16] and [17] are notable. Further extension of this algebraic approach to the entanglement[18,19] is also notable.

References

[1] Jost R, Joyeux M, Skokov S and Bowman J M 1999 *J. Chem. Phys.* **111** 6807

[2] Peterson K A, Skokov S and Bowman J M 1999 *J. Chem. Phys.* **111** 7446

[3] Joyeux M, Sugny D, Lombardi M, Jost R, Schinke R, Skokov S and Bowman J M 2000 *J. Chem. Phys.* **113** 9610

[4] Weiss J, Hauschildt J, Grebenshchikov S Y, Duren R, Schinke R, Koput J, Stamatiadis S and Farantos S C 2000 *J. Chem. Phys.* **112** 77

[5] Peterson K A 2000 *J. Chem. Phys.* **113** 4598

[6] Joyeux M, Farantos S C and Schinke R 2002 *J. Phys. Chem.* **106** A 5407

[7] Joyeux M, Grebenshchikov S Y, Bredenbeck J, Schinke R and Farantos S C 2005 *Geometric Structures of Phase Space in Multidimensional Chaos:* a special volume of advances in Chemical Physics, part A, **130** chapter 5

[8] Azzam T, Schinke R, Farantos S C, Joyeux M and Peterson K A 2003 *J. Chem. Phys.* **118** 9643

[9] Fang C and Wu G Z 2009 *Chin. Phys.* B **18** 1674

[10] Heisenberg W 1925 *Z. Physik* **33** 879

[11] Wu G Z 2005 *Nonlinearity and Chaos in Molecular Vibrations* (Amsterdam: Elsevier)

[12] Jung C and Taylor H S 2007 *J. Phys. Chem.* A **111** 3047

[13] Kellman M E 1985 *J. Chem. Phys.* **83** 3843

[14] Joyeux M, Sugny D, Tyng V, Kellman M, Ishikawa H, Field R W, Beck C and Schinke R 2000 *J. Chem. Phys.* **112** 4162

[15] Heller E J 1984 *Phys. Rev. Lett.* **53** 1515

[16] Ma Z Q, Hou X W and Xie M 1996 *Phys. Rev.* A **53** 2173

[17] Ding S and Zheng Y 1999 *J. Chem. Phys.* **111** 4466

[18] Hou X W, Chen J H and Ma Z Q 2006 *Phys. Rev.* A **74** 062513

[19] Liu Y, Zheng Y, Ren W and Ding S 2008 *Phys. Rev.* A **78** 032523